Journal of Hazardous Materials 424 (2022) 127413

Contents lists available at ScienceDirect

Journal of Hazardous Materials

journal homepage: www.elsevier.com/locate/jhazmat

Research Paper

Multiple pollution sources unravelled by environmental forensics techniques and multivariate statistics

D. Baragaño [a,*], G. Ratié [b], C. Sierra [c], V. Chrastný [b], M. Komárek [b], J.R. Gallego [a]

[a] INDUROT and Environmental Biogeochemistry & Raw Materials Group, Campus de Mieres, University of Oviedo, 33600 Mieres, Spain
[b] Department of Environmental Geosciences, Faculty of Environmental Sciences, Czech University of Life Sciences, Kamýcká 129, 16500 Prague, Czech Republic
[c] Escuela Superior de Ingenieros de Minas y Energía, Campus de Vegazana, University of León, 24071 León, Spain

ARTICLE INFO

Editor: Dr. C. LingXin

Keywords:
Toxic elements
Arsenic speciation
Lead isotopes
Polycyclic aromatic hydrocarbons
Pollution sources

ABSTRACT

Industrial sites affected by anthropogenic contamination, both past and present-day, commonly have intricate pollutant patterns, and source discrimination can be thus highly challenging. To this goal, this paper presents a novel approach combining multivariate statistics and environmental forensic techniques. The efficiency of this methodology was exemplified in a severely polluted estuarine area (Avilés, Spain), where factor analysis and clustering were performed to identify sub-areas with distinct geochemical behaviour. Once six clusters were defined and a pollution index applied, forensic tools revealed that the As speciation, Pb isotopes, and PAHs molecular ratios were useful to categorise the cluster groups on the basis of distinct pollution sources: Zn-smelting, coaly particles and waste disposal. Overall, this methodology offers valuable insight into pollution sources identification, which can be extended to comparable scenarios of complexly polluted environmental compartments. The information gathered using this approach is also important for the planning of risk assessment procedures and potential remediation strategies.

1. Introduction

The presence of multiple sources of contamination in extensive industrial areas makes it very difficult to trace the origin of contaminants. Multifaceted pollution is especially relevant in coastal areas given the importance of the ecosystems affected and the complex fate of contaminants in environmental compartments. Shorelines are sites of great ecological value and economic importance (Anbuselvan and Sridharan, 2018; Jha et al., 2019; Mossinger et al., 2013) impacted by global warming consequences (Nazarnia et al., 2020), and frequently altered by anthropogenic factors such as industrial activity, waste disposal, navigation, agricultural, and municipal uses (Kennish, 2002, 2017). The interaction of heavy industry with coastal environments leads to the release and accumulation of contaminants, among these, Potentially Toxic Elements (PTEs) and Polycyclic Aromatic Hydrocarbons (PAHs) are frequent.

PTEs (e.g., As, Cd, Cu, Cr, Hg, Pb, Zn) can be toxic even at low concentrations, mainly depending on their speciation, and are commonly monitored in mining and industry activities (Liu et al., 2020; Wu et al., 2018), including metallurgical facilities, oil combustion, power plants, and chemical manufacturing (Awasthi et al., 2017; Kowalska et al., 2018). PTEs accumulation in the environmental compartments can damage wildlife habitats by biomagnification, and can affect human health by direct exposure, e.g., dust inhalation, ingestion of contaminated water or soil/sediment, and accumulation in the food chain (Li et al., 2020; Qing et al., 2015; Zhang et al., 2014). Several technologies have been developed for removing or immobilising PTEs, in order to reduce environmental risks (Baragaño et al., 2021; Hiller et al., 2021; Kayan, 2019; Kayan and Kayan, 2021).

PAHs are hydrophobic organic pollutants, identified as carcinogens, mutagens, and teratogens (Prahl and Carpenter, 1983). They can have a natural origin, but they are also released by activities like energy production (fossil fuels), industrial operations, waste incineration, car exhausts, and biomass burning, i.e., in processes involving the incomplete combustion of organic matter (Zhang et al., 2016). When released into the atmosphere, PAHs may condensate and absorb onto particles travelling long distances (Gao et al., 2015; Zhu et al., 2014). They also tend to adsorb strongly to sediments (Pratt et al., 2012; Ramzi et al., 2017).

A clear relationship between PTEs and PAHs pollution linked to heavy industry emissions has been reported (Boente et al., 2020). This concurrent inorganic and organic contamination poses a challenge with respect to monitoring and may require customised strategies (Kruge

* Corresponding author.
E-mail address: diegobcoto@uniovi.es (D. Baragaño).

https://doi.org/10.1016/j.jhazmat.2021.127413
Received 30 June 2021; Received in revised form 20 September 2021; Accepted 30 September 2021
Available online 2 October 2021

et al., 2020). To overcome this issue, environmental forensics proposes analytical approaches combined with a detailed knowledge of the study area and its industrial history (Bonetti and Quarino, 2014; Hagmann et al., 2019; Sangwan et al., 2020; Thavamani et al., 2011). Therefore, forensics studies encompass the search for compounds, elements, isotopic signatures, and/or molecular-markers to identify distinctive features of contamination (Fernández et al., 2020; Gallego et al., 2016; Kelepertzis et al., 2020; Komárek et al., 2008; Lee et al., 2020), given that the differentiation of pollution sources is relevant from the perspective of environmental and public health. These approaches can also be supported by the application of multivariate statistical methods to differentiate between polluted and unpolluted areas, and also to identify correlations between contaminants, revealing common anthropogenic sources (Gallego et al., 2019; Reidy et al., 2013; Sierra et al., 2014).

Within this context, the goal of this research is to propose a novel integration of environmental forensic techniques and multivariate statistics, in order to disentangle the complexity of pollution sources that could be overlooked by means of other commonly used methodological approaches. This can be also useful to obtain additional data relevant to subsequent steps in the site remediation process (risk assessment, selection of remedial technologies, etc.). We thus focus on providing new

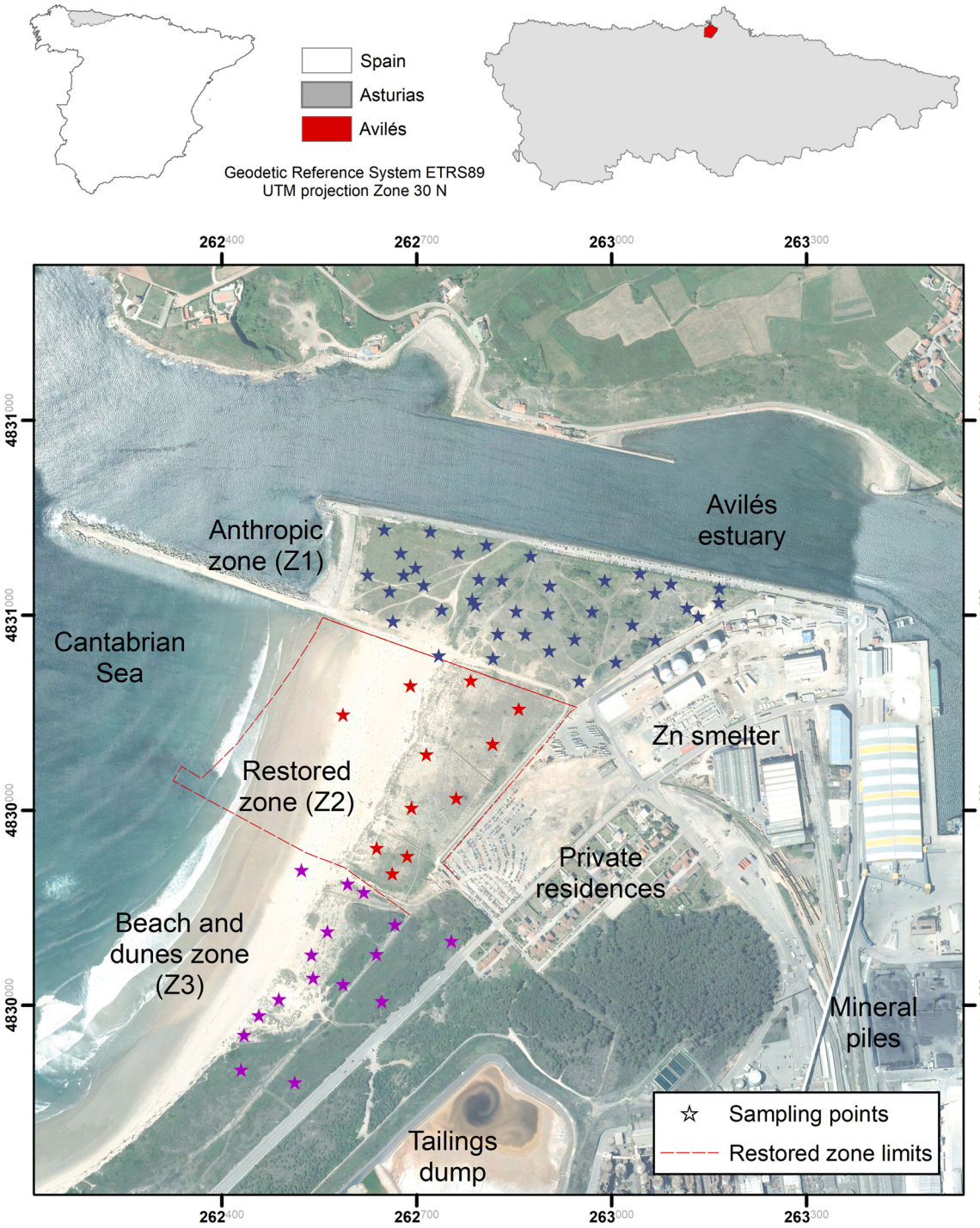

Fig. 1. Study area and samples along the three defined zones. Main industrial areas are indicated. Note also that feeding material (Fe-ores and Zn-ores) and coal are frequently stockpiled in the harbour. Other nearby industries (not included in the map) are located in an area less than 3 km to the south-east of the study area.

multidimensional insights for anthropogenic source tracing in industrial areas, rather than focusing on only a limited number of parameters or a mere quantification of usual contaminants. The industrial area and the surroundings of Avilés (Principality of Asturias, northern Spain) is a great example to demonstrate the usefulness of the proposed methodology in a polluted shoreline area.

2. Materials and methods

2.1. Site description

The study area is located in NW Spain in the surroundings of Avilés (78,000 inhabitants), a town with a large harbour and a factory belt that includes industries devoted to steel production, Zn hydrometallurgy, fertiliser production, and glass manufacturing, all located less than 5 km from an important estuary (Gallego et al., 2002; Menédez and Fernández, 2005; Sierra et al., 2014). In addition, major potential sources of diffuse pollution, including a coal power station and a second steel factory, are located less than 25 km to the east of the estuary. Evidence of PTE pollution was previously found in the area, although elements such as Hg were not monitored and organic contaminants were not considered (Gallego et al., 2002; Sierra et al., 2014). The considerable industrial activity in the area and surroundings has not decreased in recent years, which would suggest a potential increase in contamination levels (Ordóñez et al., 2015; Sanz-Prada et al., 2020). In this context, in December 2012, an accident at the Zn factory led to the release of a considerable amount of Hg (Queipo-Abad et al., 2019).

The sampling campaign focused on the left bank of the Avilés Estuary, where 3 zones were considered (Fig. 1). Covering 9.2 Ha, zone I is an area of dunes located in the mouth of the Avilés Estuary. This zone is formed mainly by natural sandy sediments mixed with anthropogenic materials such as fillers, and industrial and construction wastes of silty-sand texture. Zone II comprises the San Juan de Nieva beach and dunes that were restored in 2001 by means of a sandy refill from a nearby submarine deposit. Zone III is along the Salinas-San Juan de Nieva walking route, comprising part of the El Espartal dune system, one of the main aeolian dune systems in Spain (Flor-Blanco et al., 2013) and declared a natural monument (CMAOTI, 2006). The geological substrate in zones II and III is medium sand formed by the fragmentation of sedimentary rocks such as Triassic siltstone, Jurassic limestone, and Middle Jurassic siliceous conglomerates (Flor-Blanco et al., 2013).

2.2. Sampling and samples preparation

A total of 66 samples were collected followed a random scheme (Fig. 1); only for sampling density purposes three zones were defined on the basis of previous data (Sierra et al., 2014) and current land uses: In zone I (anthropogenic zone), 38 samples were collected, following a high sampling density of 4 samples/ha due to the observed in situ grain size heterogeneity of the materials and the evidences of debris disposal in the area (Theocharopoulos et al., 2001). For zones II (restored area) and III (dunes area), the sampling density used (28 samples in total) was lower as a result of the higher homogeneity of the sediments. Zone II was affected by different and current pollution sources due to the restoration actions, thus it was separated from zone III, which represents the dunes area without presence of coarse fragments related to industrial or mining wastes.

Specific samples of smelting slag (n = 2) and fly ash (n = 3) were collected from stock-piles situated closed to the Zn-smelter and out of zones I, II, III. These stock-piles, which are associated with Zn ore processing (Sierra et al., 2014), were disposed of in an uncontrolled manner for years during the second part of the 20th century. Finally, to gather information about the geochemical background, rock samples were also taken from the outcrops in the cliffs located on the south part of the beach.

Composite sediment samples (1 kg) were collected from the upper 20 cm with a stainless-steel auger and stored in inert plastic bags. All samples were air-dried at below 30 °C to avoid loss of Hg due to its high volatility and potential influence on PAHs determination. Samples were then sieved at 2 mm to remove vegetation, rocks, and anthropogenic particles over this size. An aliquot of each sample was milled (below 100 μm) using a RS 100 Resch mill at 500 RPM for 60 s.

2.3. Chemical composition and multivariate statistics

To determine total concentrations of Ag, Al, As, Ba, Bi, Ca, Cd, Co, Cr, Cu, Fe, Ga, Hg, K, Li, Mg, Mo, Ni, Pb, Rb, Light Rare Earths (LREE; as the sum of Ce, Eu, La, Nd, Pr, and Sm), Heavy Rare Earths (HREE; as the sum of Dy, Er, Gd, Ho, Lu, Tb, Tm and Yb), Sb, Sc, Sn, Sr, Th, Ti, Tl, U, V, Y and Zn, representative milled sub-samples of 1 g were shipped to the ISO 9002-accredited Bureau Veritas Laboratories (Vancouver, Canada). Samples were subjected to "aqua regia" digestion and the inorganic chemical composition were determined by Inductively Coupled Plasma-Mass Spectrometry (ICP-MS) using the Ultratrace AQ250 analytical package. For QA/QC purposes, five blanks (analytical and method), five duplicates, and ten analyses of standard reference materials (internal standards and OREAS45EA) were inserted into the sequences of samples to provide a measurement of background noise, accuracy, and precision.

Descriptive statistics (mean, median, standard deviation (SD), and relative standard deviation (RSD)) were obtained for all the elements analysed in the samples. Moreover, this database was subjected to a Factor Analysis employing Principal Component Analysis. Factor extraction was performed by the Kaiser/Gutmann criterion and Varimax rotation was applied to minimise the number of variables with high loadings (Reimann and De Caritat, 2005). To obtain groups of samples with similar geochemical profiles, a cluster analysis was carried out on the factor coefficient matrix as described in Gallego et al. (2019). The hierarchical procedure applied Ward's algorithm, maximising the variances between groups and minimising them between members of the same group (Murtagh and Legendre, 2014).

The Sediment Quality Index (SQI) was determined for each sample using the SQI 1.0 model, which is a modified application of the CCME Water Quality Index model (CCME, 2017, 2001). To calculate the SQI, As, Cd, Cu, Hg, Pb, and Zn concentrations and the reference values from the Predicted Effect Level (PEL) guidelines (CCME, 2001) were introduced into the model.

2.4. Environmental forensic study

For each cluster identified in the previous step, three most polluted samples (higher SQI) were selected for additional analyses to ascertain pollution sources once considered that the similarity intra-group was high enough to obtain significant results only with three samples. As an exception, one of the groups (see results) was only represented by two samples.

Particle size fractioning was performed using wet-sieving (< 125, 125–500, 500–2000 μm fractions). An enrichment factor for each of the three fractions was determined as the relationship between the PTE concentration in each fraction and that of the whole sample below 2 mm.

Mercury and As speciation was determined in a 1260 Infinity HPLC coupled to a 7700 ICPMS (Agilent Technologies) (Baragaño et al., 2020).

Lead isotopic composition (^{206}Pb, ^{207}Pb and ^{208}Pb) was determined using ICP-MS (ICapQ, Thermo Scientific, Germany). Mass bias during the determination of the Pb isotopic ratios was corrected using analyses of SRM 981 (Common lead NIST, USA) after every two samples. The standard errors for measurement of the $^{206}Pb/^{207}Pb$ and $^{208}Pb/^{206}Pb$ ratios were < 0.3% RSD and < 0.4% RSD, respectively.

For PAH determination, representative 10 g subsamples were extracted with dichloromethane: acetone (1:1) in a Soxtherm apparatus (Gerhardt). The extracts were concentrated by rotary evaporation, and the 16 priority PAHs were measured after injection into a 7890A GC

System coupled to a 5975C Inert XL MSD with a Triple-Axis Detector (Agilent Technologies) and following a modification of EPA method 8272. The chromatographic parameters used were as in Boente et al. (2020). The mass spectrometer was operated in selected ion monitoring mode (SIM), and the quantification *m/z* relations are shown in Table S1. PAHs were classified according to the molecular weight: the sum of heavy molecular weight compounds (ΣHMW) were determined comprising Naphthalene (N), Acenaphthylene (Acy), Acenaphthene (Ace), Fluorene (F), Phenanthrene (Phe), and Anthracene (Ant) concentrations; and the sum of light molecular weight compounds (ΣLMW) were calculated summing Fluoranthene (Fla), Pyrene (Pyr), Benz[*a*] anthracene (BaA), Chrysene (Chr), Benzo[*b*]fluoranthene (BbF), Benzo [*k*]fluoranthene (BkF), Benzo[*a*]pyrene (BaP), Dibenz[*a*,*h*]anthracene (DBahA), Benzo[ghi]perylene (BghiP), and Indene[1,2,3-cd]pyrene (Ipyr) concentrations. Furthermore, total ion chromatograms (TIC) of the most relevant samples were obtained in full-scan mode (mass range acquisition from 45 to 500 *m/z*) for qualitative description.

3. Results and discussion

3.1. Potentially toxic elements

Descriptive statistics of the multi-element analysis are shown in Table 1 (n = 66). Mean concentrations of As, Cd, Cu, Hg, Pb, and Zn exceeded the PEL values (Table 1). PTE data for these six elements were non-normal as the RSDs were above 50, indicating high variability and suggesting an anthropogenic input. In contrast, typically lithogenic elements, such as V or REEs, followed a normal distribution with a low RSD.

Table 1
Descriptive statistics for the elements studied: mean, standard deviation (SD), relative standard deviation (RSD), minimum (Min.) and maximum (Max.), and reference values according to PEL (CCME, 2001) guidelines for the PTEs of interest. All data are expressed in mg/kg, except g/kg for Al, Ca, Fe, K, Mg.

Element	Mean	SD	Min.	Max.	RSD (%)	PEL
Ag	1.02	1.21	0.02	7.77	119	
Al	1.01	0.43	0.45	2.15	42.2	
As	43.4	26.0	9.50	141	59.8	41.6
Ba	273	203	29.0	917	74.7	
Bi	0.94	1.01	0.16	7.05	107	
Ca	2.09	0.87	0.15	5.01	41.4	
Cd	18.3	21.7	0.34	111	119	1.20
Co	7.62	2.90	2.70	18.2	38.1	
Cr	20.2	7.84	9.00	61.0	38.8	
Cu	78.6	78.7	8.80	515	100	108
Fe	2.78	1.37	1.01	8.42	49.3	
Ga	3.20	1.01	1.56	5.70	31.7	
Hg	4.70	13.5	0.07	70.0	287	0.70
K	0.17	0.10	0.08	0.60	59.9	
Li	13.6	3.47	5.50	24.4	25.6	
Mg	0.48	0.12	0.14	0.86	25.4	
Mo	1.05	1.11	0.23	7.62	107	
Ni	18.8	7.60	7.90	51.4	40.4	
Pb	407	320	74.9	1900	78.6	112
Rb	8.98	4.74	3.80	25.8	52.8	
LREE	55.8	10.9	32.1	88.5	19.5	
HREE	4.95	1.03	2.50	7.70	20.9	
Sb	5.36	3.88	1.09	19.3	72.4	
Sc	1.86	0.59	0.80	3.50	31.8	
Sn	4.79	5.38	0.44	33.3	112	
Sr	85.5	31.4	15.1	188	36.7	
Th	3.63	1.57	0.50	7.90	43.2	
Ti	0.01	0.01	0.00	0.03	37.5	
Tl	0.22	0.28	0.03	2.20	132	
U	1.00	0.57	0.30	2.60	56.9	
V	27.8	8.20	12.0	59.0	29.5	
Y	5.66	1.50	2.53	10.9	26.6	
Zn	5310	5626	721	38400	106	271

3.2. Multivariate study

The factor analysis was initially tested using the Kaiser-Meyer-Olkin (KMO) parameter to evaluate the proportion of variance that may be caused by several factors (Cerny and Kaiser, 1977). In this case, a KMO value of 0.705 was obtained, thereby indicating good adequacy. Extraction was done using principal components followed by varimax rotation, and six factors were obtained, explaining approximately 88% of the initial variance (Table 2).

PTEs such as Cd, Cu, Hg, Pb, Tl, and Zn were well represented by Factor 1 (F1), accounting for 20.6% of the variance. The association of these pollutants is well-known in environmental geochemistry (Burton et al., 2005) and may be linked here to the Zn- smelter emissions, as previously reported (Gallego et al., 2002; Sierra et al., 2014), and also given the typical Zn ore mineralogy and the subsequent PTEs emissions in this type of metallurgical industry (Vaněk et al., 2013).

Factor 2 (F2) accounted for 19.8% of the variance and included elements related to natural and clayey or fine sand materials, such as Al, K, or Rb. This factor may be labelled as a natural input (Gallego et al., 2002). Likewise, lithogenic elements such as Sc, and REEs were represented by Factor 3 (F3), which accounted for 19.0% of the variance. This factor relates to the natural geochemical background (geogenic dust and sand) (López Peláez and Rodríguez, 2008), probably representing a second natural input.

Factor 4 (F4) accounted for 12.3% of the variance. The main elements included in this factor were Co, Cr, Mo, Ni, and Sn, which may be associated with Fe oxides and linked both to natural oxides but also to Fe metallurgy emissions, and perhaps to Fe ore dust resulting from the handling of the mineral in the harbour.

Calcareous materials are represented by Factor 5 (F5), which was less relevant, accounting for 8.9% of the variance. Elements such as Ca and Mg were the most representative in this factor.

The last factor (F6) included As and Sb and accounted for 7.9% of the variance. These two metalloids (and PTEs) commonly show a geochemical association (Fu et al., 2016; Hale, 1981) and their presence in the same isolated factor may suggest mixed origins.

The factor coefficient matrix was used to carry out a hierarchical analysis, which resulted in six geochemical clusters of samples (Fig. S1). These groups were represented geographically (Fig. 2) and the average factor loadings for the samples belonging to each one were calculated (Table S2). Concretely, group A was related to a natural factor (F3), which is consistent with the beach and restored dune area. Group B was related to F1 (Zn-Cd-Pb), which is consistent with the high PTE contents, as most of the samples included were taken near the Zn smelter. Group C was associated with the calcareous materials present in the sand of the beach and dunes (F5). Group D was linked to the notable abundance of As (F6) in a specific subarea of the anthropogenic fillers. Group (E) was linked to clayey materials (F2), probably due to the protosoil generated in the leeward zone of the dunes. Finally, group F was formed only by two outliers, which seem to be related to the Fe metallurgy (F4), probably due to the presence of slag fragments irregularly distributed in the area sampled.

3.3. Forensic study

3.3.1. As, Hg speciation and particle size distribution

A first approach to unravel the distribution of the main PTEs within the cluster groups was done using PTEs ratio (Fig. 3a), which revealed similar patterns for samples from groups A and D, whereas those of the remaining groups differed (groups B, C, E and F).

Focusing on As, samples from group D showed the highest concentrations in the area (86–293 mg/kg As) whereas those from group A were between 14 and 50 mg/kg. In this context, As speciation was determined in an attempt to discriminate between the two groups (A and D). As observed in Fig. 3(b), the higher proportion of As(V) in samples from group D, up to 96%, than in samples of group A (91%), suggested

Table 2
Factor loadings (loadings below 0.3 are omitted, between 0.3 and 0.6 should be managed prudently, higher than 0.6 marked in bold), communalities (all the elements above 0.7), and explained variance obtained after factor analysis (principal components + varimax rotation).

Variable	F1	F2	F3	F4	F5	F6	*Communality*
Zn	***.923***						*.907*
Pb	***.894***						*.873*
Tl	***.889***						*.888*
Hg	***.818***						*.697*
Cd	***.818***						*.718*
Bi	***.787***					.480	*.907*
Ag	***.783***					.420	*.963*
Cu	***.670***			.573			*.938*
Rb		***.978***					*.961*
K		***.942***					*.921*
Al		***.933***					*.947*
Li		***.738***	.396			-0.372	*.880*
Ga	.343	***.685***			-0.371		*.852*
U	.521	***.668***				.338	*.930*
Ti		***.631***	.449		.427		*.868*
V			***.925***				*.916*
LREE		.305	***.859***				*.902*
Ba			***.807***				*.765*
HREE		.433	***.804***		.325		*.944*
Sc		.390	***.776***		.394		*.918*
Th	-0.325		***.756***				*.769*
Y		.573	***.583***		.410		*.927*
Mo	.307			***.889***			*.957*
Ni			.345	***.807***			*.890*
Cr		.471		***.784***			*.956*
Co	.450		.458	***.653***			*.900*
Fe			***.644***	***.652***			*.925*
Sn		.437		***.585***		.426	*.820*
Sr					***.870***		*.886*
Ca		.304			***.867***		*.960*
Mg		.404	.502		***.546***		*.790*
As			.382			***.763***	*.847*
Sb	.319	.401				***.760***	*.882*
Var. Explained (%)	20.6	19.8	19.0	12.3	8.9	7.9	

that As derives from at least two distinct sources. Moreover, As speciation analysis of samples of ash and slag revealed that they did not contain significant As(III). This is a similar result (As(III) content < 1 mg/kg) to that obtained for the As speciation pattern of the other 4 groups (B, C, E and F). Therefore, As speciation suggests three potentially distinct As sources, one for group A, one for group D, and another one for groups B, C, E and F (mostly coincident with the As speciation in the smelter by-products). On the other hand, Hg speciation analyses revealed that Hg in all samples was fully inorganic (no methyl- or ethyl-Hg present), thus this parameter was not useful in this study.

In addition, weight proportions obtained after grain-size fractioning showed that the finer and the coarser fractions ($<$ 125 μm and 500–2000 μm) were the least abundant (fraction 500–2000 μm was even absent in some cases) and accounted for less than 10 w/w% in all samples. However, the proportion of PTEs was higher in these fractions, as revealed by enrichment ratios above 1 (Table S3). These larger contaminant loads for the least abundant fractions can be related to diffuse pollution (dust and ash) ($<$ 125 μm) and waste deposition (500–2000 μm) within the site. In fact, it is possible to identify slag and ore fragments in the coarse materials (500–2000 μm fraction), whereas medium-size particles (125–500 μm fraction) are mostly associated with geogenic particles as those found in beach and dunes.

In addition, the element ratios of the different grain-size fractions revealed opposing trends (Fig. 3(c), (d)) between the pattern of the 125–500 μm fraction and the finer fraction ($<$ 125 μm) in group A (Fig. 3 (c), (d)). In fact, the finest fraction was similar to the other samples irrespective of the group and grain-size, thereby suggesting that pollution of fine particles of group A is related to atmospheric deposition affecting the whole area, whereas the geochemical pattern of the 125–500 μm fraction is concordant with the restoration work undertaken in zone II (where samples of group A are included). Regarding the coarser fractions from groups C, D and E, high PTE concentrations are mainly a result of the presence of slags and also ore fragments.

3.3.2. *Pb isotope fingerprinting*

Several sources of Pb were foreseeable in the study area due to industrial activities (Zn-smelter but also others involving the combustion of fossil fuels) and geogenic inputs. Initially, the bedrock samples, taken from the sedimentary rock formation as a geochemical background, and the "allochthonous" waste (ash and slag) were characterised by notably distinct Pb isotopic signatures (Fig. 4). Pb isotopic ratios for the ash and slag revealed relatively homogenous compositions, and the same fingerprint was found for some of the most polluted samples. These observations thus strongly support that the main source of pollution in these samples is related to the activity of the Zn-smelter, except for group A pointing to other sources. In this regard, as reported by (Díaz-Somoano et al., 2007), the coal samples revealed a Pb isotopic fingerprint consistent with samples belonging to group A (Fig. 4), and even for some from other groups. This finding strongly suggests that coal combustion (and even coal dust) could be another source of Pb pollution. This hypothesis is supported by previous evidence of the notable influence of coal combustion on Pb content in soils in other areas of the Asturias region affected by heavy industry emissions (Boente et al., 2020, 2017). In any case, these data should be carefully managed as, in recent decades, coals from different areas of the world have also been used/managed in regional industries and harbours and this practice may modify Pb signatures (Das et al., 2018; Zhu et al., 2020).

3.3.3. *PAHs*

Most of the samples showed considerable PAH contents (above 1 mg/kg for most samples, see Table 3) with the exception of slag samples that had no PAHs. This coincides with a ΣHMW/ΣLMW ratio up to 6 revealing a pyrogenic origin for these pollutants in most of the study area, since ΣLMW compounds are usually predominant in petrogenic

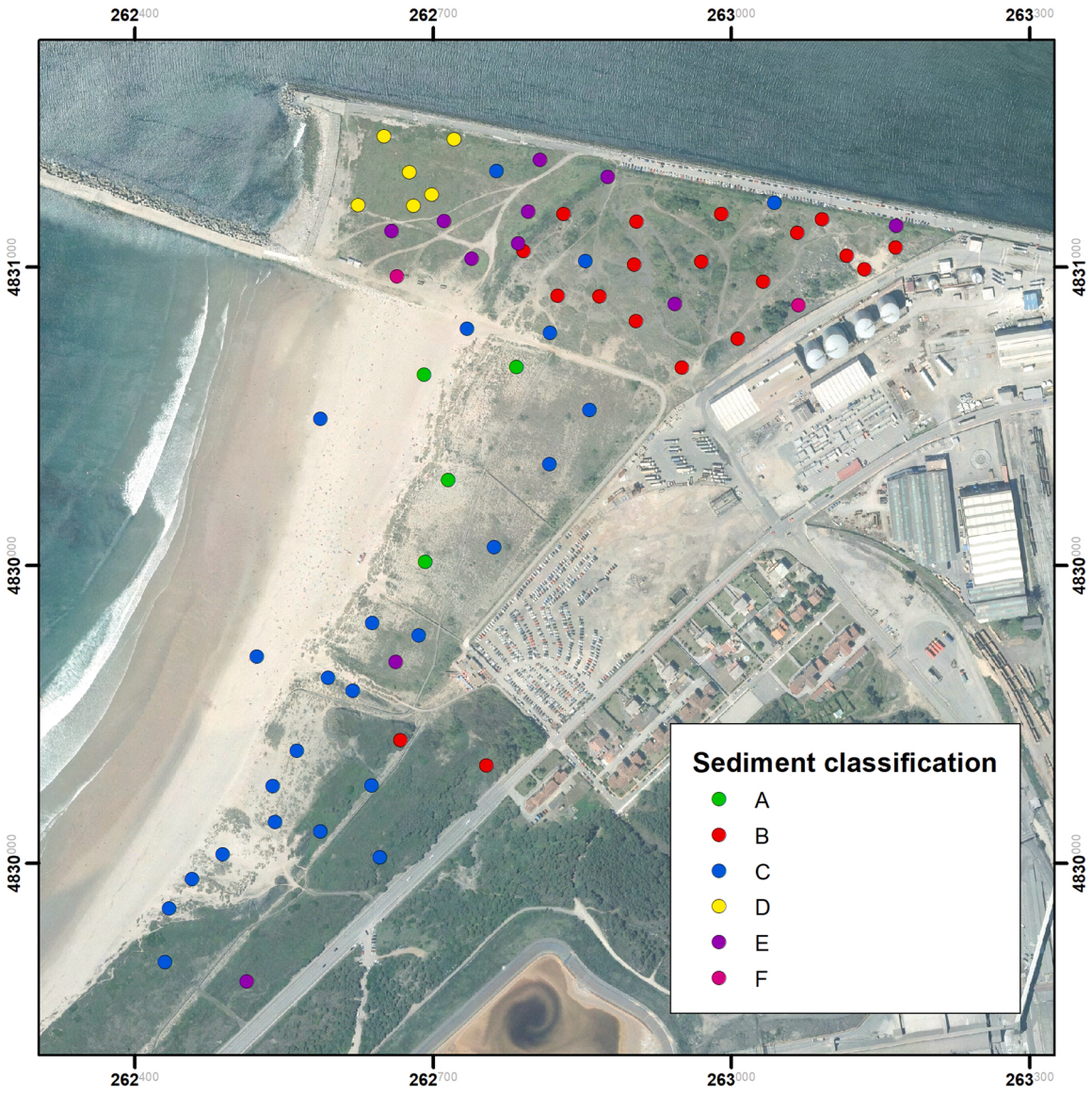

Fig. 2. Sediment classification after cluster analysis.

materials whereas ΣHMW are produced mainly by pyrolytic activities (Thiombane et al., 2019; Zhang et al., 2008). Accordingly, and consistent with the findings of Pies et al. (2008), the Ant/(Ant + Phe) ratio exceeded 0.1 for all groups and thus PAHs may derive from pyrogenic sources. Nevertheless, samples in group A had a significant lower ΣHMW/ΣLMW ratio (close to 1) than those in the other groups and also the lowest concentrations of PAHs. Moreover, ash had an average ΣHMW/ΣLMW ratio of 0.07, which is not in accordance with a pyrolytic origin. On the whole, a mixed source of pollutants can be proposed for group A samples and also for ash, as both are non-autochthonous materials in the study area and could have received a petrogenic input, such as coal dust.

Other molecular ratios reaffirmed the general hypothesis of a predominant pyrogenic source for PAHs in the study area. For example, as shown in Table 3, the Fla/(Fla + Pyr) and Ipyr/(Ipyr + BghiP) ratios were consistently above 0.5, indicating "grass, wood and coal combustion" according to De La Torre-Roche et al. (2009) and Yunker et al. (2002). Also, the BaA/(BaA + Chr) ratio (Yunker et al., 2002) showed that combustion of organic matter is the main source of PAHs (coal combustion but perhaps, in our case, also organic matter in the mineral ores treated in metallurgical processes). This is in coherence with the previous data referred and with the type of industries in the study area. To better illustrate these conclusions, cross-plots between ratios are shown in Fig. S2. Nevertheless, it should be noted that PAHs ratios have some limitations (Thiombane et al., 2019), as relative proportions of the organic compounds are usually assumed to be conserved between emission sources and the measurement points (Rocha and Palma, 2019), and they do not take into account possible alterations of the PAHs (biodegradation, burial and removal rates, etc.) as considered in Lv et al. (2020).

Finally, irrespective of molecular ratios, the concentrations of PAHs in the samples belonging to group D were significantly higher than those of the other groups (Table 3). This is another relevant feature of group D, together with the previously noted abundance of As(III), thus revealing the presence of a specific source of organic pollutants and As in the sediments included in this group (northern part of zone I, Fig. 2). TIC chromatogram showed a typical fingerprint of a coal tar distillate (Emsbo-Mattingly and Stout, 2011) with a marked abundance of heavy PAHs and the predominance of parent compounds (Fig. 5), and the absence of typical petrogenic compounds such as alkyl-PAHs (Boente et al., 2020 and references therein). This chromatogram rules out fuel spills as a source of pollution and indicates the probable release or

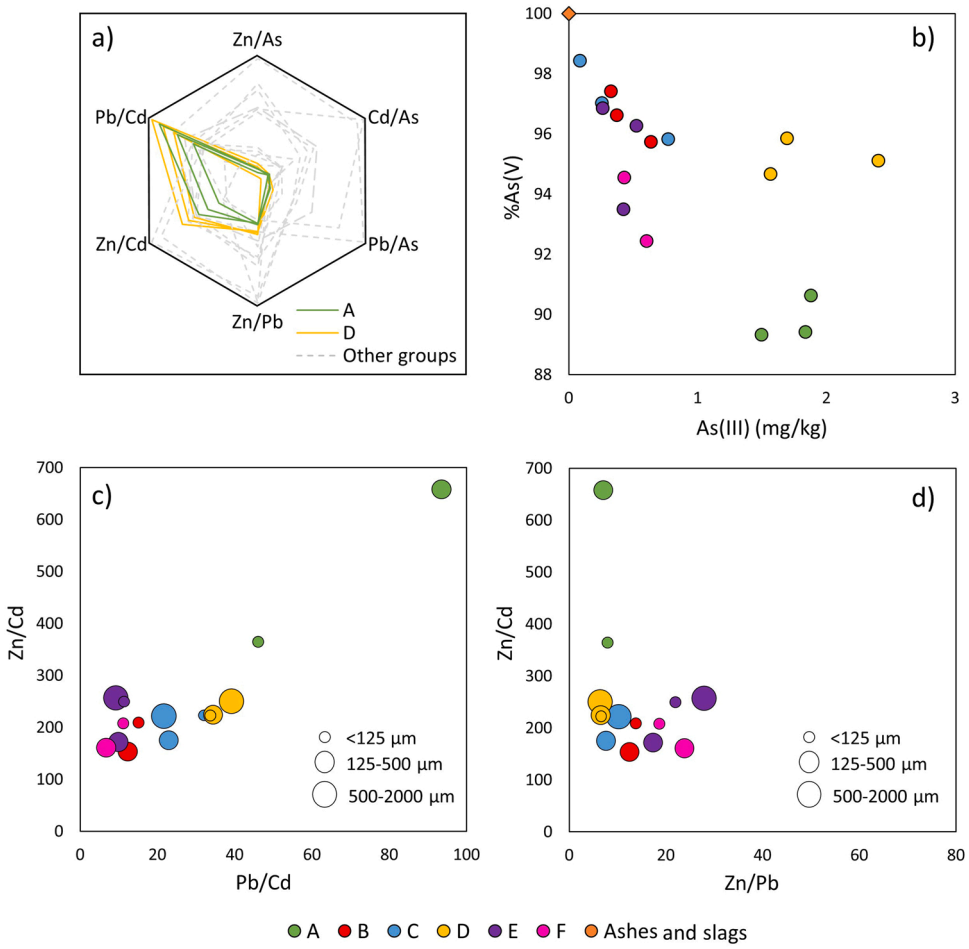

Fig. 3. Star diagrams of the element ratios of cluster samples (a); representation of samples using As speciation data (b); and geochemical ratios according to grain-size fractioning Zn/Cd vs Pb/Cd (c) and Zn/Cd vs Zn/Pb (d).

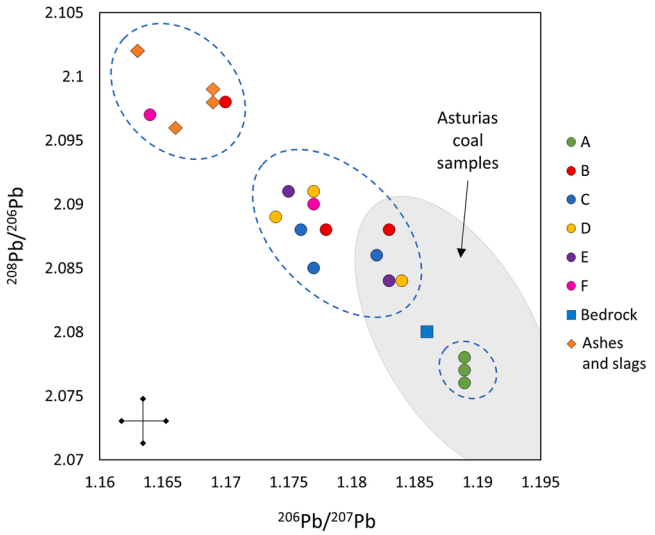

Fig. 4. Pb isotopic composition ($^{208}Pb/^{206}Pb$ vs $^{206}Pb/^{207}Pb$) of the samples collected in the study area, including sediment samples (groups A to F), bedrock, ashes and slags linked to Zn production. Error bars represent standard errors for analytical measurements. The oval indicated in grey corresponds to the intervals obtained by Díaz-Somoano et al. (2007). Leaded petrol signature corresponds to $^{206}Pb/^{207}Pb = 1.06–1.17$ and $^{208}Pb/^{206}Pb = 2.119–2.198$ according to several European studies (Kylander et al., 2005), therefore this signature is not shown in the figure.

Table 3
Sum of PAH concentrations and molecular diagnostic ratios for mean concentrations of PAHs for each cluster. RSD indicated in brackets. (Ant: Anthracene; Phe: Phenanthrene; Fla: Fluoranthene; Pyr: Pyrene; Ipyr: Indene[1,2,3-cd] pyrene; BghiP: Benzo[ghi]perylene; BaA: Benz[*a*]anthracene; Chr: Chrysene).

Parameter	Cluster groups						Ashes
	A	B	C	D	E	F	
ΣPAHs (mg/kg)	0.26 (3%)	1.2 (26%)	0.68 (20%)	43.95 (86%)	1.75 (31%)	8.15 (88%)	12.17 (70%)
ΣHMW/ΣLMW	1.25 (22%)	6.02 (14%)	6.16 (27%)	5.8 (2%)	5.74 (5%)	4.46 (12%)	4.7 (10%)
Ant/(Ant + Phe)	0.51 (3%)	0.35 (14%)	0.58 (17%)	0.22 (3%)	0.29 (21%)	0.29 (25%)	0.07 (12%)
Fla/(Fla + Pyr)	0.55 (1%)	0.56 (2%)	0.55 (2%)	0.59 (1%)	0.58 (1%)	0.58 (3%)	0.58 (4%)
Ipyr/(Ipyr + BghiP)	0.55 (1%)	0.70 (2%)	0.69 (1%)	0.76 (1%)	0.71 (3%)	0.72 (4%)	0.78 (7%)
BaA/(BaA + Chr)	0.36 (18%)	0.58 (2%)	0.52 (4%)	0.65 (2%)	0.6 (3%)	0.63 (7%)	0.64 (16%)

disposal of waste rich in pyrogenic PAHs that was superposed onto the diffuse pollution derived from coal combustion processes.

3.4. Multi-approach for pollution source tracing

Concordance between the forensic parameters described in the previous sections can be decisive for the purposes of this study; i.e., the

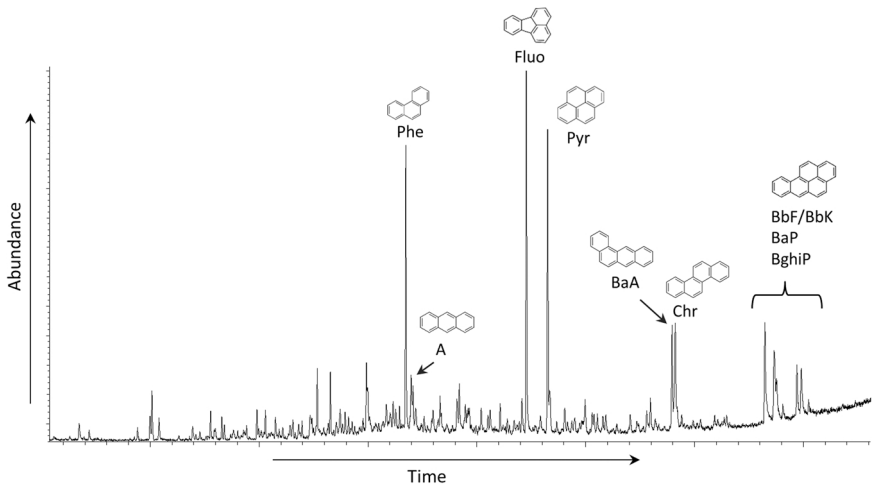

Fig. 5. Chromatogram (TIC, full-scan mode) of a representative sample of group D.

combination of data from organic pollutants analyses, Pb isotope fingerprinting and chemical speciation, can provide greater support for deciphering pollutant sources than using single technique. In this regard, a 3D representation to discriminate between groups in a single view is presented in Fig. 6 using three variables: BaA/(BaA+Chr) as a means to distinguish pyrogenic and petrogenic sources of organic pollution, the $^{206}Pb/^{207}Pb$ ratio to establish differences within sources ($^{208}Pb/^{206}Pb$ ratio reported similar results), and As speciation represented by As(III).

Using this combined-approach, samples from group A (green in Fig. 6) are clearly differentiated from the other samples as they show a notable abundance of As(III), a mixture of petrogenic and pyrogenic sources of organic pollution and a specific Pb isotopic composition. None of these three characteristics is specific to this group of samples but their combination reveals the specificity of the group. However, according to PAHs ratios, it is claimed that the influence of coal combustion particles is notable in this group. Similarly, group D was also clearly distinguished from the others because of high As(III) pollution, different Pb isotopic fingerprints and a high BaA/(BaA + Chr) ratio. The extremely high PAHs concentrations, coupled to As(III) presence and the chromatogram fingerprint (Fig. 5), suggest that pollution source corresponds to the waste disposal of a material non-related to the Zn smelter close to the site. Finally, ash samples were also clearly differentiated, whereas no significant differences were found for samples from the other group, which mostly showed the general pollution pattern of the study area; i.e. inorganic pollutants derived largely from the activities of the Zn-smelter and organic pollution caused by the emission of coal combustion. The 3D representation described here is a novel tool and can easily be adapted to other complex polluted sites.

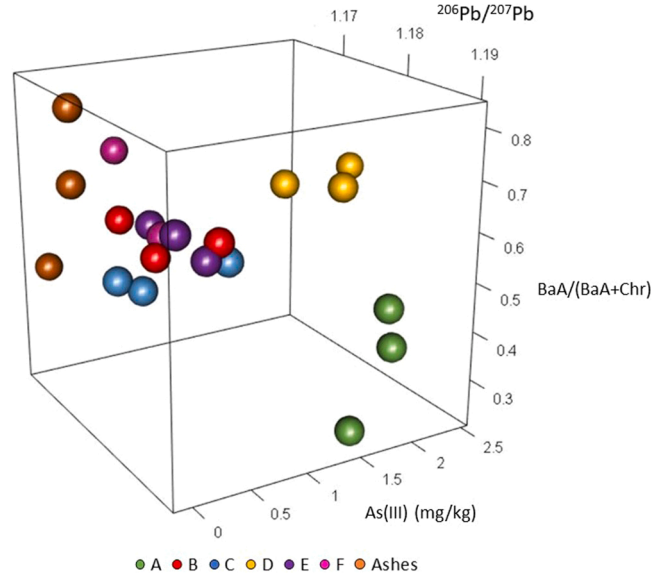

Fig. 6. Three-axis representation of the sediment and ashes samples with the contribution of PAH molecular ratios, As(III) content and $^{206}Pb/^{207}Pb$ ratio. Sediment groups A and D are clearly influenced by two specific contamination sources and differed from the other sediment group samples, which are closely together influenced by the Zn smelter, since these are closer to ashes fingerprint.

4. Conclusions

Environmental forensic studies can distinguish between pollution sources in areas with complex contamination profiles, thereby going beyond the quantification of contaminants or single geochemical ratios. In this context, we propose an approach consisting of a novel combination of multivariate statistics and forensic techniques applicable in zones affected by diverse, inorganic (PTEs) and organic (PAHs), point-source and diffuse pollution sources.

This methodology was tested in the coastal area of Avilés (Spain), where heavy industrial activity has led to a mixture of anthropogenic and natural sediments. Factor analysis and a subsequent hierarchical clustering led to the establishment of six groups of samples, whereas grain-size distribution determined that pollution affected mostly the finest fractions. After a selection of specific samples using a pollution index (SQI in our case), a more in-depth examination of the pollution sources was achieved by As speciation, Pb isotopes and organic pollutants (molecular markers of PAHs) determinations. Aggregate three-axis representation of the referred parameters permitted differentiation of diverse pollution sources, and it also provided an understanding of local features, such as Zn-smelter emissions, waste disposal or deposition of coaly particles.

In general, the main contribution of this study is a powerful combination of tools providing a multifaceted approach useful to understand pollution complex scenarios (see flowchart in Fig. S3), thereby providing a valuable insight into pollution sources identification. Likewise, this approach can be easily extended to similar sites, and may support risk assessment and selection of remediation technologies.

CRediT authorship contribution statement

D. Baragaño: Conceptualization, Methodology, Data curation,

Formal analysis, Writing – original draft. **G. Ratié:** Methodology, Data curation, Formal analysis, Writing – review & editing. **C. Sierra:** Conceptualization, Writing – review & editing. **V. Chrastný:** Formal analysis, Writing – review & editing. **M. Komárek:** Supervision, Resources, Writing – review & editing. **J.R. Gallego:** Conceptualization, Supervision, Resources, Writing – review & editing.

Declaration of Competing Interest

The authors declare that they have no known competing financial interests or personal relationships that could have appeared to influence the work reported in this paper.

Acknowledgements

This work was partially funded by the Czech Science Foundation (project No. 19-15405S) and by the project NANOCAREM (AEI/Spain, FEDER/EU, MCI-20-PID2019-106939GB-I00). Diego Baragaño obtained a grant from the "Ayudas complementarias para beneficiarios de ayudas (FPU): Estancias Breves y Traslados Temporales" program, nº. EST19/00030, financed by the "Ministerio de Educación y Formación Profesional" of Spain. We would like to thank the Environmental Assay Unit of the Scientific and Technical Services of the University of Oviedo for its technical support. The authors thank 6 anonymous reviewers for improving the quality of the paper.

Appendix A. Supplementary material

Supplementary data associated with this article can be found in the online version at doi:10.1016/j.jhazmat.2021.127413.

References

Anbuselvan, N., D, Senthil Nathan, Sridharan, M., 2018. Heavy metal assessment in surface sediments off Coromandel Coast of India: implication on marine pollution. Mar. Pollut. Bull. https://doi.org/10.1016/j.marpolbul.2018.04.074.

Awasthi, M.K., Liao, R., Ali, A., Mahar, A., Guo, D., Li, R., Xining, S., Awasthi, M.K., Wang, Q., Zhang, Z., 2017. Spatial distribution and risk assessment of heavy metals in soil near a Pb/Zn smelter in Feng County, China. Ecotoxicol. Environ. Saf. https://doi.org/10.1016/j.ecoenv.2017.01.044.

Baragaño, D., Alonso, J., Gallego, J.R., Lobo, M.C., Gil-Díaz, M., 2020. Zero valent iron and goethite nanoparticles as new promising remediation techniques for As-polluted soils. Chemosphere 238, 124624. https://doi.org/10.1016/j.chemosphere.2019.124624.

Baragaño, D., Gallego, J.L.R., María Menéndez-Aguado, J., Marina, M.A., Sierra, C., 2021. As sorption onto Fe-based nanoparticles and recovery from soils by means of wet high intensity magnetic separation. Chem. Eng. J. 408, 127325 https://doi.org/10.1016/j.cej.2020.127325.

Boente, C., Matanzas, N., García-González, N., Rodríguez-Valdés, E., Gallego, J.R., 2017. Trace elements of concern affecting urban agriculture in industrialized areas: a multivariate approach. Chemosphere 183, 546–556. https://doi.org/10.1016/j.chemosphere.2017.05.129.

Boente, C., Baragaño, D., Gallego, J.R., 2020. Benzo[a]pyrene sourcing and abundance in a coal region in transition reveals historical pollution, rendering soil screening levels impractical. Environ. Pollut. 266, 115341 https://doi.org/10.1016/j.envpol.2020.115341.

Bonetti, J., Quarino, L., 2014. Comparative forensic soil analysis of new jersey state parks using a combination of simple techniques with multivariate statistics. J. Forensic Sci. 59, 627–636. https://doi.org/10.1111/1556-4029.12375.

Burton, E.D., Phillips, I.R., Hawker, D.W., 2005. Geochemical partitioning of copper, lead, and zinc in benthic, estuarine sediment profiles. J. Environ. Qual. 34, 263–273. https://doi.org/10.2134/jeq2005.0263.

CCME, 2017. Canadian Water Quality Guidelines for the Protection of Aquatic Life: CCME Water Quality Index, User's Manual – 2017 Update, Canadian Water Quality Guidelines for the Protection of Aquatic Life.

CCME, 2001. Canadian Water Quality Guidelines for the Protection of Aquatic Life: CCME Water Quality Index 1.0, Canadian Water Quality Guidelines for the Protection of Aquatic Life.

Cerny, B.A., Kaiser, H.F., 1977. A study of a measure of sampling adequacy for factor-analytic correlation matrices. Multivar. Behav. Res. 12, 43–47. https://doi.org/10.1207/s15327906mbr1201_3.

CMAOTI, 2006. Decreto 81/2006, de 29de junio, de la Consejería de medio ambiente, ordenación del territorio einfraestructuras. Boletín Oficial del Principado de Asturias del 21 de julio de2006.

Das, A., Patel, S.S., Kumar, R., Krishna, K.V.S.S., Dutta, S., Saha, M.C., Sengupta, S., Guha, D., 2018. Geochemical sources of metal contamination in a coal mining area in Chhattisgarh, India using lead isotopic ratios. Chemosphere 197, 152–164. https://doi.org/10.1016/j.chemosphere.2018.01.016.

De La Torre-Roche, R.J., Lee, W.Y., Campos-Díaz, S.I., 2009. Soil-borne polycyclic aromatic hydrocarbons in El Paso, Texas: analysis of a potential problem in the United States/Mexico border region. J. Hazard. Mater. 163, 946–958. https://doi.org/10.1016/j.jhazmat.2008.07.089.

Díaz-Somoano, M., Suárez-Ruiz, I., Alonso, J.I.G., Ruiz Encinar, J., López-Antón, M.A., Martínez-Tarazona, M.R., 2007. Lead isotope ratios in Spanish coals of different characteristics and origin. Int. J. Coal Geol. 71, 28–36. https://doi.org/10.1016/j.coal.2006.05.006.

Emsbo-Mattingly, S.D., Stout, S.A., 2011. Semivolatile hydrocarbon residues of coal and coal tar. Coal and Peat Fires: A Global Perspective. https://doi.org/10.1016/B978-0-444-52858-2.00011-6.

Fernández, B., Lara, L.M., Menéndez-Aguado, J.M., Ayala, J., García-González, N., Salgado, L., Colina, A., Gallego, J.L.R., 2020. A multi-faceted, environmental forensic characterization of a paradigmatic brownfield polluted by hazardous waste containing Hg, As, PAHs and dioxins. Sci. Total Environ. 726, 138546 https://doi.org/10.1016/j.scitotenv.2020.138546.

Flor-Blanco, G., Flor, G., Pando, L., 2013. Evolution of the Salinas-El Espartal and Xagó beach/dune systems in north-western Spain over recent decades: evidence for responses to natural processes and anthropogenic interventions. Geo-Mar. Lett. 33, 143–157. https://doi.org/10.1007/s00367-012-0301-3.

Fu, Z., Wu, F., Mo, C., Deng, Q., Meng, W., Giesy, J.P., 2016. Comparison of arsenic and antimony biogeochemical behavior in water, soil and tailings from Xikuangshan, China. Sci. Total Environ. 539, 97–104. https://doi.org/10.1016/j.scitotenv.2015.08.146.

Gallego, J.L.R., Ordóñez, A., Loredo, J., 2002. Investigation of trace element sources from an industrialized area (Avilés, northern Spain) using multivariate statistical methods. Environ. Int. 27, 589–596. https://doi.org/10.1016/S0160-4120(01)00115-5.

Gallego, J.L.R., Ortiz, J.E., Sánchez-Palencia, Y., Baragaño, D., Borrego, Á.G., Torres, T., 2019. A multivariate examination of the timing and accumulation of potentially toxic elements at Las Conchas bog (NW Spain). Environ. Pollut. 254, 113048 https://doi.org/10.1016/j.envpol.2019.113048.

Gallego, J.R., Rodríguez-Valdés, E., Esquinas, N., Fernández-Braña, A., Afif, E., 2016. Insights into a 20-ha multi-contaminated brownfield megasite: an environmental forensics approach. Sci. Total Environ. 563–564, 683–692. https://doi.org/10.1016/j.scitotenv.2015.09.153.

Gao, B., Wang, X.M., Zhao, X.Y., Ding, X., Fu, X.X., Zhang, Y.L., He, Q.F., Zhang, Z., Liu, T.Y., Huang, Z.Z., Chen, L.G., Peng, Y., Guo, H., 2015. Source apportionment of atmospheric PAHs and their toxicity using PMF: impact of gas/particle partitioning. Atmos. Environ. 103, 114–120. https://doi.org/10.1016/j.atmosenv.2014.12.006.

Hagmann, D.F., Kruge, M.A., Cheung, M., Mastalerz, M., Gallego, J.L.R., Singh, J.P., Krumins, J.A., Li, X.N., Goodey, N.M., 2019. Environmental forensic characterization of former rail yard soils located adjacent to the Statue of Liberty in the New York/New Jersey harbor. Sci. Total Environ. 690, 1019–1034. https://doi.org/10.1016/j.scitotenv.2019.06.495.

Hale, M., 1981. Pathfinder applications of arsenic, antimony and bismuth in geochemical exploration. J. Geochem. Explor. 15, 307–323. https://doi.org/10.1016/0375-6742(81)90071-6.

Hiller, E., Jurkovič, Ľ., Faragó, T., Vítková, M., Tóth, R., Komárek, M., 2021. Contaminated soils of different natural pH and industrial origin: the role of (nano) iron- and manganese-based amendments in As, Sb, Pb, and Zn leachability. Environ. Pollut. 285, 117268 https://doi.org/10.1016/j.envpol.2021.117268.

Jha, D.K., Ratnam, K., Rajaguru, S., Dharani, G., Devi, M.P., Kirubagaran, R., 2019. Evaluation of trace metals in seawater, sediments, and bivalves of Nellore, southeast coast of India, by using multivariate and ecological tool. Mar. Pollut. Bull. 146, 1–10. https://doi.org/10.1016/j.marpolbul.2019.05.044.

Kayan, A., 2019. Inorganic-organic hybrid materials and their adsorbent properties. Adv. Compos. Hybrid Mater. 2, 34–45. https://doi.org/10.1007/s42114-018-0073-y.

Kayan, G.Ö., Kayan, A., 2021. Composite of natural polymers and their adsorbent properties on the dyes and heavy metal ions. J. Polym. Environ. 29, 3477–3496. https://doi.org/10.1007/s10924-021-02154-x.

Kelepertzis, E., Argyraki, A., Chrastný, V., Botsou, F., Skordas, K., Komárek, M., Fouskas, A., 2020. Metal(loid) and isotopic tracing of Pb in soils, road and house dusts from the industrial area of Volos (central Greece). Sci. Total Environ. 725, 138300 https://doi.org/10.1016/j.scitotenv.2020.138300.

Kennish, M.J., 2002. Environmental threats and environmental future of estuaries. Environ. Conserv. 29, 78–107. https://doi.org/10.1017/S0376892902000061.

Kennish, M.J., 2017. Estuaries: Anthropogenic Impacts. Springer, Cham, pp. 1–9. https://doi.org/10.1007/978-3-319-48657-4_140-2.

Komárek, M., Ettler, V., Chrastný, V., Mihaljevič, M., 2008. Lead isotopes in environmental sciences: a review. Environ. Int. 34, 562–577. https://doi.org/10.1016/j.envint.2007.10.005.

Kowalska, J.B., Mazurek, R., Gąsiorek, M., Zaleski, T., 2018. Pollution indices as useful tools for the comprehensive evaluation of the degree of soil contamination–a review. Environ. Geochem. Health 40, 2395–2420. https://doi.org/10.1007/s10653-018-0106-z.

Kruge, M.A., Lara-Gonzalo, A., Gallego, J.L.R., 2020. Environmental forensics of complexly contaminated sites: a complimentary fingerprinting approach. Environ. Pollut. 263, 114645 https://doi.org/10.1016/j.envpol.2020.114645.

Kylander, M.E., Weiss, D.J., Martínez Cortízas, A., Spiro, B., Garcia-Sanchez, R., Coles, B. J., 2005. Refining the pre-industrial atmospheric Pb isotope evolution curve in Europe using an 8000 year old peat core from NW Spain. Earth Planet. Sci. Lett. 240, 467–485. https://doi.org/10.1016/j.epsl.2005.09.024.

Lee, P.K., Kang, M.J., Jeong, Y.J., Kwon, Y.K., Yu, S., 2020. Lead isotopes combined with geochemical and mineralogical analyses for source identification of arsenic in agricultural soils surrounding a zinc smelter. J. Hazard. Mater. 382, 121044 https://doi.org/10.1016/j.jhazmat.2019.121044.

Li, X., Zhang, J., Gong, Y., Liu, Q., Yang, S., Ma, J., Zhao, L., Hou, H., 2020. Status of copper accumulation in agricultural soils across China (1985–2016). Chemosphere. https://doi.org/10.1016/j.chemosphere.2019.125516.

Liu, J., Wei, X., Zhou, Y., Tsang, D.C.W., Bao, Z., Yin, M., Lippold, H., Yuan, W., Wang, J., Feng, Y., Chen, D., 2020. Thallium contamination, health risk assessment and source apportionment in common vegetables. Sci. Total Environ. https://doi.org/10.1016/j.scitotenv.2019.135547.

López Peláez, J., Rodríguez, G. Flor, 2008. Evolución ambiental del estuario de Avilés (1833-2006). Trab. Geol. 119–135. https://doi.org/10.17811/tdg.28.2008.

Lv, M., Luan, X., Liao, C., Wang, D., Liu, D., Zhang, G., Jiang, G., Chen, L., 2020. Human impacts on polycyclic aromatic hydrocarbon distribution in Chinese intertidal zones. Nat. Sustain. 3, 878–884. https://doi.org/10.1038/s41893-020-0565-y.

Menédez, M., Fernández, B., 2005. Industrial park remediation in aviles. Miner. Energy Raw Mater. Rep. https://doi.org/10.1080/14041040510042301.

Mossinger, J., White, M., Goymer, P., 2013. Coastal regions. Nature 504, 35. https://doi.org/10.1038/504035a.

Murtagh, F., Legendre, P., 2014. Ward's hierarchical agglomerative clustering method: which algorithms implement ward's criterion? J. Classif. 31, 274–295. https://doi.org/10.1007/s00357-014-9161-z.

Nazarnia, H., Nazarnia, M., Sarmasti, H., Wills, W.O., 2020. A systematic review of civil and environmental infrastructures for coastal adaptation to sea level rise. Civ. Eng. J. 6, 1375–1399. https://doi.org/10.28991/cej-2020-03091555.

Ordóñez, A., Álvarez, R., De Miguel, E., Charlesworth, S., 2015. Spatial and temporal variations of trace element distribution in soils and street dust of an industrial town in NW Spain: 15 years of study. Sci. Total Environ. 524–525, 93–103. https://doi.org/10.1016/j.scitotenv.2015.04.024.

Pies, C., Hoffmann, B., Petrowsky, J., Yang, Y., Ternes, T.A., Hofmann, T., 2008. Characterization and source identification of polycyclic aromatic hydrocarbons (PAHs) in river bank soils. Chemosphere 72, 1594–1601. https://doi.org/10.1016/j.chemosphere.2008.04.021.

Prahl, F.G., Carpenter, R., 1983. Polycyclic aromatic hydrocarbon (PAH)-phase associations in Washington coastal sediment. Geochim. Cosmochim. Acta 47, 1013–1023. https://doi.org/10.1016/0016-7037(83)90231-4.

Pratt, B., Riesen, R., Johnston, C.G., 2012. PLFA analyses of microbial communities associated with PAH-contaminated riverbank sediment. Microb. Ecol. 64, 680–691. https://doi.org/10.1007/s00248-012-0060-8.

Qing, X., Yutong, Z., Shenggao, L., 2015. Assessment of heavy metal pollution and human health risk in urban soils of steel industrial city (Anshan), Liaoning, Northeast China. Ecotoxicol. Environ. Saf. 120, 377–385. https://doi.org/10.1016/j.ecoenv.2015.06.019.

Queipo-Abad, S., González, P.R., Martínez-Morillo, E., Davis, W.C., García Alonso, J.I., 2019. Concentration of mercury species in hair, blood and urine of individuals occupationally exposed to gaseous elemental mercury in Asturias (Spain) and its comparison with individuals from a control group formed by close relatives. Sci. Total Environ. 672, 314–323. https://doi.org/10.1016/j.scitotenv.2019.03.367.

Ramzi, A., Habeeb Rahman, K., Gireeshkumar, T.R., Balachandran, K.K., Jacob, C., Chandramohanakumar, N., 2017. Dynamics of polycyclic aromatic hydrocarbons (PAHs) in surface sediments of Cochin estuary, India. Mar. Pollut. Bull. 114, 1081–1087. https://doi.org/10.1016/j.marpolbul.2016.10.015.

Reidy, L., Bu, K., Godfrey, M., Cizdziel, J.V., 2013. Elemental fingerprinting of soils using ICP-MS and multivariate statistics: a study for and by forensic chemistry majors. Forensic Sci. Int. 233, 37–44. https://doi.org/10.1016/j.forsciint.2013.08.019.

Reimann, C., De Caritat, P., 2005. Distinguishing between natural and anthropogenic sources for elements in the environment: regional geochemical surveys versus enrichment factors. Sci. Total Environ. 337, 91–107. https://doi.org/10.1016/j.scitotenv.2004.06.011.

Rocha, A.C., Palma, C., 2019. Source identification of polycyclic aromatic hydrocarbons in soil sediments: application of different methods. Sci. Total Environ. 652, 1077–1089. https://doi.org/10.1016/j.scitotenv.2018.10.014.

Sangwan, P., Nain, T., Singal, K., Hooda, N., Sharma, N., 2020. Soil as a tool of revelation in forensic science: a review. Anal. Methods 12, 5150–5159. https://doi.org/10.1039/d0ay01634a.

Sanz-Prada, L., García-Ordiales, E., Roqueñí, N., Grande Gil, J.A., Loredo, J., 2020. Geochemical distribution of selected heavy metals in the Asturian coastline sediments (North of Spain). Mar. Pollut. Bull. 156, 111263 https://doi.org/10.1016/j.marpolbul.2020.111263.

Sierra, C., Boado, C., Saavedra, A., Ordóñez, C., Gallego, J.R., 2014. Origin, patterns and anthropogenic accumulation of potentially toxic elements (PTEs) in surface sediments of the Avilés estuary (Asturias, northern Spain). Mar. Pollut. Bull. 86, 530–538. https://doi.org/10.1016/j.marpolbul.2014.06.052.

Thavamani, P., Megharaj, M., Krishnamurti, G.S.R., McFarland, R., Naidu, R., 2011. Finger printing of mixed contaminants from former manufactured gas plant (MGP) site soils: implications to bioremediation. Environ. Int. 37, 184–189. https://doi.org/10.1016/j.envint.2010.08.017.

Theocharopoulos, S.P., Wagner, G., Sprengart, J., Mohr, M.E., Desaules, A., Muntau, H., Christou, M., Quevauviller, P., 2001. European soil sampling guidelines for soil pollution studies. Sci. Total Environ. 264, 51–62. https://doi.org/10.1016/S0048-9697(00)00611-2.

Thiombane, M., Albanese, S., Di Bonito, M., Lima, A., Zuzolo, D., Rolandi, R., Qi, S., De Vivo, B., 2019. Source patterns and contamination level of polycyclic aromatic hydrocarbons (PAHs) in urban and rural areas of Southern Italian soils. Environ. Geochem. Health 41, 507–528. https://doi.org/10.1007/s10653-018-0147-3.

Vaněk, A., Chrastný, V., Komárek, M., Penížek, V., Teper, L., Cabala, J., Drábek, O., 2013. Geochemical position of thallium in soils from a smelter-impacted area. J. Geochem. Explor. 124, 176–182. https://doi.org/10.1016/j.gexplo.2012.09.002.

Wu, W., Wu, P., Yang, F., Ling Sun, D., Zhang, D.X., Zhou, Y.K., 2018. Assessment of heavy metal pollution and human health risks in urban soils around an electronics manufacturing facility. Sci. Total Environ. https://doi.org/10.1016/j.scitotenv.2018.02.183.

Yunker, M.B., Macdonald, R.W., Vingarzan, R., Mitchell, R.H., Goyette, D., Sylvestre, S., 2002. PAHs in the Fraser River basin: a critical appraisal of PAH ratios as indicators of PAH source and composition. Org. Geochem. 33, 489–515. https://doi.org/10.1016/S0146-6380(02)00002-5.

Zhang, C., Gang Yu, Z., Ming Zeng, G., Jiang, M., Zhu Yang, Z., Cui, F., Ying Zhu, M., Qing Shen, L., Hu, L., 2014. Effects of sediment geochemical properties on heavy metal bioavailability. Environ. Int. 73, 270–281. https://doi.org/10.1016/j.envint.2014.08.010.

Zhang, W., Zhang, S., Wan, C., Yue, D., Ye, Y., Wang, X., 2008. Source diagnostics of polycyclic aromatic hydrocarbons in urban road runoff, dust, rain and canopy throughfall. Environ. Pollut. 153, 594–601. https://doi.org/10.1016/j.envpol.2007.09.004.

Zhang, Y., Lin, Y., Cai, J., Liu, Y., Hong, L., Qin, M., Zhao, Y., Ma, J., Wang, X., Zhu, T., Qiu, X., Zheng, M., 2016. Atmospheric PAHs in North China: spatial distribution and sources. Sci. Total Environ. https://doi.org/10.1016/j.scitotenv.2016.05.104.

Zhu, Y., Yang, L., Yuan, Q., Yan, C., Dong, C., Meng, C., Sui, X., Yao, L., Yang, F., Lu, Y., Wang, W., 2014. Airborne particulate polycyclic aromatic hydrocarbon (PAH) pollution in a background site in the North China Plain: concentration, size distribution, toxicity and sources. Sci. Total Environ. https://doi.org/10.1016/j.scitotenv.2013.07.030.

Zhu, Z., Li, Z., Wang, S., Bi, X., 2020. Magnetic mineral constraint on lead isotope variations of coal fly ash and its implications for source discrimination. Sci. Total Environ. 713, 136320 https://doi.org/10.1016/j.scitotenv.2019.136320.